Research Square

Preprints are preliminary reports that have not undergone peer review. They should not be considered conclusive, used to inform clinical practice, or referenced by the media as validated information.

Zinc-Nicotinic Acid MOFs Wrapped in Polyaniline: Streamlined Synthesis and Bifunctional Electrocatalytic Performance

Hussain S. AlShahrani
King Abdulaziz University
Hadi M. Marwani
King Abdulaziz University
Khalid A Alzahrani
King Abdulaziz University
Anish Khan
akrkhan@kau.edu.sa

King Abdulaziz University

Research Article

Keywords: MOF, Nanocomposite, Polymer, Metal, Green Energy, HER, OER

Posted Date: October 16th, 2026

DOI: https://doi.org/10.21203/rs.3.rs-11129371/v1

License: This work is licensed under a Creative Commons Attribution 4.0 International License. Read Full License

Additional Declarations: No competing interests reported.

Abstract

The escalating global energy demand, driven by rapid industrialization and population growth, continues to pose a significant challenge to the scientific community. The prevailing dependence on fossil fuels has exacerbated environmental deterioration and public health risks, necessitating a decisive shift toward sustainable energy alternatives. Among these, hydrogen production via water electrolysis has emerged as a promising pathway, particularly when enabled by advanced catalytic materials. In this study, we report the development of a novel PANI@Zn-NA-MOF nanocomposite catalyst, synthesized via a sol-gel approach, which strategically integrates conductive polymers with metal–organic frameworks to enhance electrochemical performance. The as-prepared catalyst was thoroughly characterized using a variety of analytical techniques. Surface morphology and elemental composition were examined via scanning electron microscopy coupled with energy-dispersive X-ray spectroscopy (SEM-EDX). Structural elucidation was performed using Fourier-transform infrared (FTIR) spectroscopy to identify chemical bonds and functional groups, while ultraviolet–visible (UV-Vis) spectroscopy provided insight into optical absorption properties. Thermal stability was evaluated through thermogravimetric analysis (TGA), and surface chemical states were analyzed via X-ray photoelectron spectroscopy (XPS).

Morphological analysis revealed that PANI@Zn-NA-MOF exhibits a nanocapsular architecture. TGA results demonstrated outstanding thermal stability, with only approximately 2.5% weight loss observed up to 550°C. The appearance of a single characteristic peak in the UV-Vis spectrum confirmed the successful formation of the composite. Furthermore, FTIR and XPS analyses confirmed the presence of expected functional groups and elemental signatures, validating the successful integration of Zn within the MOF framework. Notably, the PANI@Zn-NA-MOF composite exhibited remarkable electrocatalytic efficiency toward water splitting, requiring an overpotential of only 0.47 V to drive the electrolysis process. When measured against the reversible hydrogen electrode (RHE), the catalyst delivered onset potentials of 1.6 V/RHE for the oxygen evolution reaction (OER) and 0.2 V/RHE for the hydrogen evolution reaction (HER). This impressive performance significantly reduces the energy input required for electrolysis, thereby enhancing the feasibility of large-scale hydrogen production. Given that hydrogen combustion produces only water as a byproduct, the development of such high-performance catalysts represents a meaningful step forward in the transition toward clean and sustainable energy systems.

1. Introduction

The relentless rise in global energy consumption, coupled with the pressing reality of climate change, has made it unequivocally clear that our continued reliance on fossil fuels is no longer a viable option. The urgent need to transition toward sustainable and environmentally benign energy sources has never been more apparent [1]. Among the various alternatives being explored, hydrogen has emerged as a particularly attractive energy carrier. With a remarkable energy density of 142 MJ kg^{-1}, hydrogen offers substantial power output while producing only water as a combustion byproduct rendering it a truly zero-emission fuel [2, 3]. This raises a fundamental question: how can hydrogen be produced in a clean and sustainable manner? Among the available routes, electrochemical water splitting has garnered

considerable attention, particularly when driven by renewable energy sources such as solar or wind power [4, 5]. The water electrolysis process comprises two essential half-reactions: the hydrogen evolution reaction (HER) occurring at the cathode and the oxygen evolution reaction (OER) taking place at the anode. However, the overall water-splitting reaction ($2H_2O \rightarrow 2H_2 + O_2$) is thermodynamically unfavourable, demanding a significant energy input of 237.2 kJ mol^{-1}, which corresponds to a theoretical potential of 1.23 V per electron. To overcome the substantial kinetic barriers and drive the reaction at practically viable rates, the deployment of efficient electrocatalysts becomes necessary [6, 7].

Currently, the benchmark electrocatalysts for water splitting continue to be noble-metal-based materials. Platinum (Pt) and its alloys remain the gold standard for the HER, while iridium oxide (IrO_2) and ruthenium oxide (RuO_2) are widely regarded as the most effective OER catalysts [8, 9]. Nevertheless, the practical implementation of these materials in large-scale industrial electrolyzers is severely hampered by their exorbitant costs, extreme scarcity, and often insufficient long-term operational stability [10, 11]. These inherent limitations have galvanized a worldwide research effort aimed at developing highly efficient, durable, and cost-effective electrocatalysts derived from earth-abundant elements [12, 13].

Interestingly, significant progress has been made in replacing precious metals with more abundant alternatives. A wide array of materials has been investigated to date, including transition metal oxides [14, 15], hydroxides [16], phosphides [17, 18], sulfides [19, 20], selenides [21], nitrides [22], and carbides [23] all of which have demonstrated promising electrocatalytic potential. For instance, NiFe layered double hydroxides have shown OER performance in alkaline media that rivals that of noble metal oxides [24]. Similarly, nickel phosphide (Ni_2P) and cobalt phosphide (CoP) have emerged as outstanding bifunctional catalysts capable of driving both HER and OER efficiently, a property that is believed to originate from their favorable hydrogen binding energies [25]. However, despite these encouraging developments, several challenges remain unresolved. Issues such as nanoparticle agglomeration, insufficient exposure of active sites, and limited long-term durability continue to impede the widespread adoption of these materials in practical applications [26].

Meanwhile, metal–organic frameworks better known as MOFs have emerged as a fresh and exciting direction in the field of electrocatalysis. Constructed from metal nodes interconnected by organic linkers, these porous materials offer an impressive degree of tunability that researchers are eager to exploit [27, 28]. These architectures are formed by linking metal ions or clusters through organic linker molecules, which spontaneously self-assemble into well-ordered crystalline networks, creating structured frameworks with one-, two-, or three-dimensional topologies [29]. Their exceptional characteristics include extraordinarily high specific surface areas (sometimes exceeding 7000 m^2 g^{-1}), adjustable pore dimensions, and, most importantly, the capacity for precise molecular-level control over their chemical and structural properties [30, 31]. This inherent tunability paves the way for the rational design of catalytic active sites, which can significantly enhance both activity and selectivity [32].

Zinc-based MOFs are particularly promising in this field. Zinc is an inexpensive and readily available transition metal that exhibits favorable electrochemical properties and offers versatile coordination

geometries, traits that are highly advantageous for catalytic applications [33]. Furthermore, the flexible coordination environment of zinc ions can give rise to distinct structural features that may function as effective catalytic centers for both HER and OER [34]. By employing a straightforward organic linker such as nicotinic acid (isonicotinic acid), it becomes possible to construct stable Zn-MOFs designed with open metal sites and functional groups capable of participating in proton-coupled electron transfer processes a fundamental mechanism at the heart of water-splitting reactions [35].

However, the direct application of pristine MOFs in electrocatalysis is frequently hindered by two major shortcomings: their inherently poor electrical conductivity and limited stability in aqueous electrolyte media, particularly under operational potentials [36, 37]. Most MOFs behave as electrical insulators, as electrons remain localized between the metal clusters and organic linkers, thereby impeding efficient charge transport throughout the material during catalytic processes [38]. This poor conductivity can obscure the intrinsic activity of the catalytic sites, ultimately leading to elevated overpotentials and sluggish reaction kinetics [39]. Although strategies such as developing two-dimensional conductive MOFs or incorporating redox-active linkers have been explored to address this issue, their synthesis routes are often difficult to scale up for practical applications [40].

A practical and effective approach to circumvent the conductivity bottleneck involves the integration of MOFs with highly conductive materials, thereby constructing composite architectures that harness the synergistic advantages of both components [41]. Conducting polymers are particularly well-suited for this role. Materials such as polyaniline, polypyrrole, and PEDOT, which feature extended π-conjugated backbones, exhibit efficient electrical conductivity. They also demonstrate good stability under diverse conditions, are relatively straightforward to synthesize, and have been extensively investigated in the literature [42]. Among these conducting polymers, polyaniline (PANI) stands out due to its unique doping chemistry, excellent aqueous stability, and low cost [43]. The combination of MOFs with PANI yields composites that capitalize on the strengths of both constituents: the MOF contributes its high surface area and precisely defined active sites, while PANI provides a robust and continuous network for rapid charge transport [44]. The intimate interfacial contact between the MOF and PANI facilitates efficient electron transfer into the MOF particles, effectively wiring them to the electrode and ensuring full utilization of their active sites [45]. Moreover, the porous structure of the MOF can effectively prevent the agglomeration of PANI chains, thereby preserving a large electrochemically active surface area [46].

The synthetic route employed for the fabrication of the composite plays a pivotal role in determining its final physicochemical properties and overall electrocatalytic performance. Simple physical blending approaches frequently result in poor interfacial contact and heterogeneous mixtures, which severely undermine the synergistic effects between components [47]. In contrast, the sol-gel technique offers a superior bottom-up strategy for the construction of hybrid materials [48]. This process essentially involves the transformation of a liquid sol comprising suspended colloidal particles into a solid gel network through controlled hydrolysis and condensation reactions. The principal advantages of this method for producing MOF-polymer composites are substantial. First, it enables molecular-level mixing, wherein the precursors are homogeneously combined in solution, yielding a uniform distribution of the

constituent phases [49]. Second, it promotes enhanced interfacial interactions, as the in-situ formation of one component within the other fosters strong chemical and physical bonding, which is critical for efficient charge transfer across the interface [50]. Moreover, the sol-gel approach provides exceptional control over the morphological features, allowing for the fine-tuning of textural properties such as porosity and particle size by simply adjusting synthesis parameters including pH, temperature, and precursor concentration [51]. An additional advantage is that the process operates under mild conditions, frequently at or near room temperature, thereby preserving the structural integrity of sensitive frameworks that might otherwise be compromised under harsh synthetic conditions [52].

Based on these design principles, the present study is dedicated to the development and systematic evaluation of a novel bifunctional electrocatalyst capable of efficiently driving both half-reactions of overall water splitting. This goal is achieved through the strategic integration of a zinc-based metal–organic framework with a conductive polyaniline network. The MOF selected for this purpose is constructed from zinc ions and nicotinic acid (NA), chosen on the basis of its promising catalytic activity and structural robustness. This Zn-NA-MOF was subsequently combined with PANI via an optimized sol-gel synthesis protocol, yielding a composite material denoted as PANI@Zn-NA-MOF. The overarching aim is to fabricate a hybrid system that effectively overcomes the inherent limitations of its individual components. Specifically, we anticipate that the PANI matrix will form a highly conductive percolation network throughout the MOF structure, thereby substantially enhancing charge transport kinetics during electrocatalytic operation. Concurrently, the Zn-NA-MOF component is expected to provide a wealth of readily accessible catalytic active sites while simultaneously mitigating the aggregation of PANI chains, thus preserving a large electrochemically active surface area. Through this synergistic interplay, the two constituents are anticipated to generate a composite material with markedly improved electrocatalytic performance and long-term operational stability toward both the hydrogen evolution reaction (HER) and oxygen evolution reaction (OER) under alkaline conditions. Following synthesis, the PANI@Zn-NA-MOF composite was subjected to a comprehensive characterization campaign encompassing detailed structural, morphological, and electrochemical investigations. The material was then rigorously evaluated to ascertain its true bifunctional electrocatalytic efficacy, and the findings unequivocally reveal its considerable promise for practical deployment in advanced water-splitting technologies.

2.Experimental

2.1. Reagents and Apparatus

All chemical reagents employed in this study including aniline, hydrochloric acid (HCl), ammonium persulfate ($(NH_4)_2S_2O_8$), nicotinic acid, zinc acetate, ethylene glycol, and Nafion were procured from Sigma-Aldrich (USA). All reagents were of analytical grade and were utilized as received without any further purification. To comprehensively characterize the synthesized materials, a broad array of analytical techniques was employed. Surface morphology was examined using a TESCAN MIRA3 field-emission scanning electron microscope (FE-SEM, TESCAN, Czech Republic). Functional groups were identified via Fourier-transform infrared (FTIR) spectroscopy using a Thermo Scientific Nicolet iS20

spectrometer (Thermo Fisher Scientific, USA). Ultraviolet-visible (UV-Vis) absorption spectra were recorded on a Shimadzu UV-2600 spectrophotometer (Shimadzu Corporation, Japan). Thermogravimetric analysis (TGA) was conducted using a TA Instruments Q50 thermogravimetric analyzer (TA Instruments, USA), while X-ray photoelectron spectroscopy (XPS) measurements were performed on a Kratos Axis Supra spectrometer (Kratos Analytical Ltd, UK). All electrochemical measurements for water splitting were carried out using a PalmSens EmStat4S potentiostat in a standard three-electrode cell configuration. The working electrode consisted of either a bare glassy carbon electrode (GCE, 1.3 mm diameter) or a GCE modified with the PANI@Zn-NA-MOF composite. An Ag/AgCl electrode (saturated with 3 M KCl) served as the reference electrode, and a platinum wire (1 mm diameter) was used as the counter electrode.

2.2. Preparation of PANI@Zn-NA-MOF Nanocomposite

2.2.1. Synthesis of Polyaniline

Polyaniline (PANI) was synthesized via the oxidative polymerization of aniline monomer. A series of aniline monomer solutions with concentrations of 1%, 3%, 5%, and 7% (v/v) were prepared in 1 M hydrochloric acid (HCl) using separate 250 mL conical flasks. In parallel, a 1 M standard stock solution of ammonium persulfate (APS), serving as the oxidizing agent, was also prepared in 1 M HCl. For each polymerization reaction, a fixed volume (50 mL) of the APS solution was added dropwise to each of the 1%, 3%, 5%, and 7% aniline monomer solutions in a 250 mL conical flask placed in an ice bath to maintain the temperature at 5°C. The mixture was continuously stirred for 2 hours. The addition rate was meticulously controlled to ensure the formation of a homogeneous mixture. The appearance of a dark greenish-black color indicated the successful formation of the emeraldine salt form of PANI (PANI-ES). Subsequently, the reaction flask was stored in a refrigerator overnight to allow the polymerization process to proceed to completion.

2.2.2. Synthesis of Zinc-Based Metal–Organic Framework (Zn-NA-MOF)

The zinc-based metal–organic framework (Zn-NA-MOF) was synthesized according to a previously reported procedure with minor modifications [53]. In a typical synthesis, 0.123 g (1 mmol) of nicotinic acid (NA) and 0.109 g (0.5 mmol) of zinc(II) acetate dihydrate were each dissolved separately in 20 mL of a mixed solvent composed of deionized water and ethylene glycol in a 1:1 (v/v) ratio. Both solutions were heated and stirred at 80°C for 10 minutes. Subsequently, the zinc acetate solution was rapidly added to the NA solution under vigorous stirring at 1000 rpm. After 10 minutes of intense agitation, the resulting mixture was centrifuged at 7000 rpm. The obtained solid precipitate was washed three times with deionized water at 60°C and three times with absolute ethanol to eliminate any residual impurities. Finally, the purified product was dried using a freeze-drying (lyophilization) technique, yielding a white powder, which was subsequently stored at 4°C for future use.

2.2.3. Synthesis of PANI@Zn-NA-MOF Nanocomposite

The pre-synthesized polyaniline slurries and the as-prepared Zn-NA-MOF were slowly mixed together in a 500 mL conical flask under gentle stirring for 1 hour in an ice-cold bath. The resulting mixture was then kept in a refrigerator at a temperature below 5°C for 24 hours, with the pH carefully maintained below 5 through the dropwise addition of dilute hydrochloric acid solution. After 24 hours, the obtained product was filtered using Whatman filter paper on a Büchner funnel. The collected solid was thoroughly washed with deionized water and ethanol until all impurities were completely removed. Finally, the purified composite was dried in an oven overnight at an appropriate temperature, ready for subsequent characterization and application.

2.2.4. Electrical Conductivity Behavior of the PANI@Zn-NA-MOF Nanocomposite

To prepare the composite sample for electrical conductivity measurements, the as-synthesized material was first purified by washing with a 1 M hydrochloric acid (HCl) solution, followed by thorough rinsing with deionized water to eliminate any residual acid traces. The cleaned sample was then dried in an oven at a temperature ranging between 40 and 50°C until complete dryness was achieved. Subsequently, 200 mg of the dried material was finely ground using an agate mortar and pestle to obtain a homogeneous powder. The resulting powder was then pressed into pellets at ambient temperature using a hydraulic press under a compressive force of 25 kN, which was maintained for 20 minutes to ensure proper compaction. The thickness of each pellet was precisely measured using a micrometer to ensure accuracy in subsequent calculations. Finally, the electrical conductivity of the pellets was determined using a standard four-probe or two-probe method, depending on the setup. Based on the obtained conductivity values, the sample exhibiting the highest electrical conductivity was selected for further characterization and application studies.

2.3. Characterization

The as-synthesized PANI@Zn-NA-MOF composite was thoroughly characterized using a comprehensive suite of analytical techniques. To examine the crystalline structure and degree of crystallinity of the materials, X-ray diffraction (XRD) analysis was performed using an Arl Xtra diffractometer equipped with a Cu-Kα radiation source (λ = 1.5406 Å). Data were collected across a 2θ range of 15–80° at a scanning rate of 5° min^{-1}. Scanning electron microscopy (SEM) was employed to investigate the surface morphology and elemental composition using a JEOL JSM-7600F instrument, which was equipped with an energy-dispersive X-ray spectroscopy (EDX) detector from Oxford Instruments for elemental identification. Furthermore, surface chemical analysis was conducted using X-ray photoelectron spectroscopy (XPS) on a Kα 1 spectrometer, which provided detailed information regarding the elemental constituents and their respective chemical binding states using a monochromatic Al Kα X-ray source (1486.6 eV). Meanwhile, functional groups including metal–oxygen (M–O) bonds were identified via Fourier-transform infrared (FTIR) spectroscopy using a Thermo-Scientific instrument. The electrochemical properties of the composite were evaluated using two complementary techniques. Electrochemical impedance spectroscopy (EIS) was carried out over a frequency range spanning from 100 kHz to 1 mHz, and the resulting data were fitted to an equivalent electrical circuit using Autolab EIS

software. Cyclic voltammetry (CV) was also performed across a potential window of 0 to 1.0 V at a scan rate of 100 mV s^{-1} with a step potential of 8 mV. All electrochemical measurements were conducted using a PalmSens EmStat4S potentiostat to gain insight into electron mobility and the overall electrochemical behavior of the composite material.

2.4. Water Splitting Studies

The electrocatalytic water-splitting performance of the synthesized composite was systematically evaluated through electrochemical measurements, with the general experimental conditions detailed in Section 2.1. For the preparation of the electrocatalyst working electrode, 100 µg of the as-synthesized PANI@Zn-NA-MOF composite was dispersed in a 10% ethanolic solution. The resulting dispersion was then deposited onto the surface of a glassy carbon electrode (GCE), which had been pre-coated with a single drop of liquid Nafion to serve as a binder. The electrochemical performance was assessed using linear sweep voltammetry (LSV) to acquire current–voltage polarization profiles.

For the oxygen evolution reaction (OER) performance evaluation, measurements were conducted in a 1 M KOH aqueous solution that had been pre-purged with oxygen to ensure saturation. Linear sweep voltammetry (LSV) was performed by sweeping the potential from 0.6 V to 1.8 V (vs. Ag/AgCl) at a scan rate of 100 mV s^{-1}, with a step potential of 8 mV and an AC amplitude of 5 mV. The hydrogen evolution reaction (HER) activity was evaluated in an acidic medium of 0.5 M H_2SO_4. In the alkaline medium (1 M KOH), the potential was scanned from 0 V to -1.5 V (vs. Ag/AgCl) at a scan rate of 100 mV s^{-1}, with an AC amplitude of 5 mV and a step potential of 8 mV. All measured potentials were subsequently converted to the reversible hydrogen electrode (RHE) scale using the Nernst equation, where E_{RHE} and $E_{Ag/AgCl}$ represent the potentials versus RHE and the Ag/AgCl reference electrode, respectively.

3. Results and Discussion

In this study, we successfully synthesized a PANI@Zn-NA-MOF nanocomposite using the well-established sol-gel method and thoroughly characterized it employing a range of spectrophotometric and analytical techniques. The unique physicochemical properties of the as-prepared material positioned it as a promising candidate for energy-related applications. Consequently, we utilized this composite to fabricate an electrode for electrochemical water splitting. The catalytic activity of the fabricated electrode was subsequently investigated through systematic electrochemical testing, encompassing both the oxygen evolution reaction (OER) and the hydrogen evolution reaction (HER).

3.1. Morphological Characterization

Morphological characterization was performed using scanning electron microscopy (SEM) analysis, as presented in Fig. 1. The micrographs revealed that the PANI@Zn-NA-MOF nanocomposite consists of a heterogeneous mixture of nanostructures with distinct morphologies at various magnifications. At higher resolution, the images displayed well-defined nanocrystals with clearly identifiable edges and facets. These well-developed crystalline features are of particular significance, as they serve as potential

active centers for catalytic reactions. Moreover, in conjunction with the presence of oxygen vacancies (O-vacancies), these structural features facilitate efficient electron transport between the catalyst surface and the electrolyte, thereby enhancing the overall electrocatalytic performance. These observations collectively confirm that the adopted sol-gel synthesis strategy successfully yielded high-quality, well-defined nanocrystals with desirable morphological characteristics for electrocatalytic applications.

Fourier-transform infrared (FTIR) spectroscopy was performed to verify the successful formation of the PANI@Zn-NA-MOF composite and to elucidate the intermolecular interactions between its constituent components, as shown in Fig. 2a. The spectrum revealed characteristic absorption bands that confirm the presence of both the Zn-based metal–organic framework and the polyaniline network [53]. The peaks observed at 724 and 752 cm^{-1} are attributed to out-of-plane C–H bending vibrations of the benzene ring, which are common to both the nicotinic acid linker and the polyaniline structure [54, 55]. The distinct peaks at 844 and 896 cm^{-1} confirm the presence of out-of-plane C–H bending vibrations characteristic of a disubstituted benzene ring, a signature feature of the polyaniline backbone [56]. The absorption bands appearing in the region of 1195–1264 cm^{-1} arise from C–N stretching vibrations associated with the benzenoid and quinoid units of the PANI chain, further confirming its successful incorporation [57]. A peak observed at 1362 cm^{-1} is assigned to the C = N stretching vibration originating from the quinoid segments of the polymer structure [55]. The most pronounced and diagnostic features of the spectrum are the intense peaks centered at 1517 cm^{-1} and 1626 cm^{-1}, which correspond to the C = C and C = N stretching vibrations of the aromatic rings present in both the MOF linker and the polyaniline backbone [53, 56]. Collectively, the FTIR data provide compelling evidence that the composite was successfully synthesized as intended. Furthermore, the spectrum suggests the existence of π–π stacking interactions, and possibly hydrogen bonding, between the Zn-NA-MOF framework and the conductive PANI polymer, indicating strong interfacial interactions that are crucial for efficient charge transfer.

Thermogravimetric analysis (TGA) was performed to evaluate the thermal stability of the PANI@Zn-NA-MOF composite, and the resulting curve is presented in Fig. 2b. The TGA profile reveals that the composite exhibits outstanding thermal stability, with the mass remaining largely unchanged up to approximately 580°C. The initial minor weight loss observed below 150°C is attributed to the desorption of physically adsorbed water molecules and residual solvent from the surface of the material [57]. A more pronounced weight loss occurs in the temperature range of 250–400°C, which corresponds to the thermal decomposition of the polyaniline polymer chains [58]. Subsequently, a sharp decline in mass is observed between 400 and 580°C, associated with the degradation of the organic linker (nicotinic acid) within the Zn-NA-MOF framework [57]. The final residual mass, amounting to approximately 1.9% at elevated temperatures, indicates the formation of stable inorganic residues, most likely zinc oxide (ZnO), which confirms the hybrid organic–inorganic nature of the synthesized composite. This remarkable thermal stability, extending up to 580°C, positions the PANI@Zn-NA-MOF composite as a promising candidate for applications requiring robust performance under high-temperature conditions.

The ultraviolet-visible (UV-Vis) absorption spectrum of the PANI@Zn-NA-MOF composite, presented in Fig. 2c, provides compelling evidence for the successful formation of the hybrid material and offers valuable insights into its electronic structure. A distinctive absorption band centered at approximately 430 nm is observed, which serves as a definitive signature of polaronic transitions, characteristic of the conductive emeraldine salt form of polyaniline (PANI-ES). The presence of this feature unequivocally confirms that PANI exists in its highly conductive state within the composite. Furthermore, a broad absorption tail extending from the visible region into the near-infrared range is clearly visible, indicating strong electronic interactions between the PANI matrix and the Zn-NA-MOF framework. These interactions are likely attributable to metal-to-ligand charge transfer (MLCT) processes and π–π stacking interactions at the intimate interface between the two components. This effective electronic coupling, combined with a relatively narrow optical band gap, endows the composite with promising photoresponsive properties. These characteristics position the PANI@Zn-NA-MOF composite as a highly promising candidate for visible-light-driven applications, including photocatalytic processes and solar energy conversion technologies.

Energy-dispersive X-ray spectroscopy (EDX) was employed to verify the elemental composition of the synthesized PANI@Zn-NA-MOF composite, and the resulting spectrum is presented in Fig. 2d. The analysis provides clear and unambiguous evidence for the successful integration of all constituent components. The spectrum reveals a dominant presence of carbon (61.32 wt%) and nitrogen (21.04 wt%), which are the primary elemental constituents of the polyaniline (PANI) backbone and the nicotinic acid organic linker, respectively. The notably high nitrogen content serves as a particularly strong indicator of the successful incorporation of PANI into the composite structure. Furthermore, the detection of oxygen (15.64 wt%) is consistent with the carboxylate functional groups present in the nicotinic acid linker. Most importantly, the definitive signal corresponding to zinc (1.04 wt%) conclusively confirms the presence of the zinc-based metal–organic framework (Zn-NA-MOF) within the hybrid material. This collective elemental signature, which distinctly showcases the key elements derived from both the conducting polymer and the MOF component, provides direct and compelling evidence for the successful formation of the intended PANI@Zn-NA-MOF hybrid composite.Furthermore, the spectrum reliably detected oxygen at 16.60 wt%, a finding fully consistent with the expected chemical structure. This oxygen is attributable to the carboxylate ($-COO^-$) functional groups that coordinate with the metal centers in the Zn-NA-MOF, forming the essential bonds of the framework itself. Most critically, the definitive spectroscopic signal for zinc was observed at 1.04 wt%. This unambiguous detection of the metal center validates the presence of the zinc-based secondary building units that form the inorganic nodes of the metal-organic framework.

X-ray photoelectron spectroscopy (XPS) analysis was performed to investigate the surface chemical composition and oxidation states of the PANI@Zn-NA-MOF composite, and the corresponding spectra are presented in Fig. 3. The survey scan spectrum clearly confirms the presence of zinc (Zn), nitrogen (N), carbon (C), and oxygen (O) as the primary elemental constituents, providing compelling evidence for the successful formation of the composite. The high-resolution Zn 2p spectrum (Fig. 3d) exhibits two characteristic spin-orbit splitting peaks at binding energies of 1045.0 eV (Zn $2p_{1/2}$) and 1022.0 eV (Zn

$2p_{3/2}$), which are in excellent agreement with the Zn^{2+} oxidation state, confirming the presence of zinc ions within the metal–organic framework structure. The N 1s spectrum (Fig. 3c) can be deconvoluted into three distinct components: a quinonoid imine (= N-) peak at approximately 398.5 eV, a benzenoid amine (-NH-) peak at around 399.5 eV, and a positively charged nitrogen (N^+) species at approximately 401.0 eV. This deconvolution pattern is characteristic of the emeraldine salt form of polyaniline, confirming that PANI exists in its highly conductive state within the composite. The high-resolution C 1s spectrum displays multiple peaks corresponding to C–C/C = C bonds at 284.8 eV, C–N bonds at 285.8 eV, and C = O bonds at 288.5 eV, which originate from both the PANI backbone and the nicotinic acid organic linker. The O 1s region reveals two distinct components: a peak at approximately 531.5 eV attributed to metal–oxygen (Zn–O) bonds, and a second peak at around 533.0 eV corresponding to oxygen atoms within carbonyl (C = O) groups. The absence of any extraneous peaks in the XPS spectra confirms the high phase purity of the synthesized material. Furthermore, the specific binding energies and the characteristic deconvolution pattern of the nitrogen components provide strong evidence for successful interfacial interactions between PANI and the Zn-NA-MOF framework, likely arising from coordination bonding and π–π stacking interactions.

3.2. Electrical Conductivity Study

The electrical conductivity of pellets fabricated from the PANI@Zn-NA-MOF composite was evaluated using the four-point probe technique, a highly reliable and widely adopted method for determining the conductivity of semiconducting materials. This technique is strongly preferred over conventional two-probe methods as it effectively circumvents inherent limitations, including rectifying effects commonly encountered at metal–semiconductor interfaces and the injection of minority carriers by one of the contacts. Such phenomena can artificially shift the potential at other contacts and compromise the accuracy of conductance readings, thereby undermining the reliability of the measurements. To determine the electrical conductivity of the composite samples, the following equations were applied: The corrected electrical resistivity (ρ) was determined using Eq. (1):

$\rho = \rho_0 \times G_7(W/S)$ (1)

where:

ρ represents the corrected resistivity (Ω·cm)

ρ_0 denotes the uncorrected resistivity (Ω·cm)

$G_7(W/S)$ is the geometric correction factor employed when the bottom surface is non-conducting.

This correction factor depends on:

W: the thickness of the sample (cm)

S: the spacing between the measurement probes (cm)

The specific relationships are defined as follows:

The correction factor is given by Eq. (2):

$G_7(W/S) = (2S/W) \times \ln(2)$ (2)

The uncorrected resistivity is calculated using Eq. (3):

$\rho_o = (V/I) \times 2\pi S$ (3)

Finally, the electrical conductivity (σ) is obtained from Eq. (4):

$\sigma = 1/\rho$ (4)

The electrical conductivity of the prepared pellets was systematically measured using the four-point probe technique. To optimize the composite's performance, a series of samples were synthesized with varying polyaniline content (1%, 2%, 5%, and 7%) while maintaining a constant Zn-NA-MOF concentration. The electrical characterization revealed a distinct optimal composition, with the sample containing 5% polyaniline exhibiting a peak conductivity of approximately 43,6 S/cm. This value was substantially higher than those observed for composites with either lower (1% and 2%) or higher (7%) PANI loadings. This result underscores that achieving an optimal balance between the conducting polymer and the MOF components is critical for maximizing electrical performance. In this particular system, the 5% PANI formulation proved to be the most effective in establishing a continuous and efficient conductive network throughout the composite structure, thereby facilitating enhanced charge transport.

3.3. Catalytic Study

3.3.1. Oxygen Evolution Reaction of PANI@ZnNA-MOF catalyst

To evaluate the OER performance of the synthesized PANI@ZnNA-MOF catalyst, the supporting electrolyte was first optimized. Linear sweep voltammetry (LSV) was conducted in three different media: 1 M NaOH, 1 M H_2SO_4, and a buffer solution, as shown in Fig. 4a. Among these, 1 M NaOH exhibited significantly superior performance, characterized by a remarkably low onset potential of approximately 1.45 V vs. RHE and the ability to achieve a massive current density of 3000 mA/cm² at a relatively low overpotential. In sharp contrast, the acidic 1 M H_2SO_4 medium required a much higher potential (exceeding 2.0 V vs. RHE) to yield a modest current response, confirming the kinetic limitations of water oxidation in acidic environments due to the scarcity of hydroxyl ions. Consequently, the alkaline 1 M NaOH medium was selected as the optimal electrolyte for all subsequent electrochemical tests, as it provides an abundant supply of OH^- ions to efficiently drive the forward OER kinetics.

The intrinsic electrocatalytic activity of PANI@ZnNA-MOF was compared to bare GCE, pure PANI, and pristine ZnNA in 1 M NaOH, as depicted in Fig. 4b. The PANI@ZnNA-MOF electrode displayed

exceptional activity, reaching a benchmark current density of 10 mA/cm² at a low applied potential of 1.55 V vs. RHE. Under the same potential, the bare GCE exhibited negligible current density (< 0.5 mA/cm²), while pure PANI and ZnNA achieved current densities of approximately 2.5 mA/cm² and 4 mA/cm², respectively. This drastic enhancement underscores a profound synergistic effect between PANI and the ZnNA-MOF components, resulting in far superior OER activity compared to its individual constituents.

The enhanced performance is fundamentally linked to the electrode's real electrochemically active surface area (ECSA). The relationship between the scan rate and current density was analyzed from Figs. 4c and 4d. By plotting the current density variation (Δj) against the scan rate, the double-layer capacitance (Cdl*Cdl*) was calculated to be a substantial 329.4 mF/cm². Considering that a flat electrode typically exhibits a Cdl*Cdl* of ~ 30 μF/cm², the estimated roughness factor is approximately 10,980. Based on the electrode's geometric area, this translates to an enormous ECSA for the PANI@ZnNA-MOF layer, far exceeding that of the bare GCE. Such a massive active surface area provides abundant catalytic active sites, facilitating highly efficient anion and charge exchange at the electrode-electrolyte interface, which is pivotal for the superior OER activity.

Electrochemical impedance spectroscopy (EIS) was employed to investigate the electrode kinetics, as illustrated in the Nyquist plots in Fig. 4e. The charge transfer resistance (*Rct*), which corresponds to the diameter of the semicircle, was significantly reduced for the PANI@ZnNA-MOF electrode. While the bare GCE displayed a very large *Rct* (> 10,000 Ω), the modified electrode demonstrated a remarkably lower *Rct* of approximately 6,000 Ω. This dramatic reduction in charge transfer resistance confirms that the PANI@ZnNA-MOF composite possesses excellent electrical conductivity, enabling faster electron transfer kinetics during the OER process.

Finally, the long-term durability of the PANI@ZnNA-MOF catalyst was examined via chronopotentiometry at a constant current density of 10 mA/cm² for 5000 seconds (Fig. 4f). The catalyst exhibited outstanding stability, maintaining a stable operating potential of approximately 1.55 V throughout the entire 5000-second test with virtually no potential shift or degradation. This robust structural and electrochemical stability highlights the PANI@ZnNA-MOF as a highly reliable and durable electrocatalyst, making it a promising, cost-effective candidate for sustainable energy conversion systems.

3.3.2. Hydrogen evolution reaction (HER) activity of PANI@ZnNA-MOF catalyst

In Fig. 5a, a control study conducted in 1 M NaOH compares the HER performance of the PANI@ZnNA-MOF modified electrode with bare GCE, pure PANI, and pristine ZnNA. The PANI@ZnNA-MOF electrode delivered a benchmark current density of 10 mA/cm² at a remarkably low overpotential, significantly outperforming its individual components. In contrast, the bare GCE exhibited negligible current density even at highly negative potentials. Furthermore, both pristine PANI and ZnNA required substantially

higher applied potentials to achieve 10 mA/cm², highlighting the strong synergistic effect between the polyaniline matrix and the ZnNA framework in the composite catalyst.

To determine the electrochemically active surface area (ECSA), cyclic voltammetry was performed in the non-Faradaic region at various scan rates, as shown in Fig. 5b. The linear relationship between the current density difference and the scan rate is plotted in Fig. 5c. A linear fit of the data points yielded a slope of 0.0775. Using the established formula

$$C_{dl}=|slope|/2$$

The double-layer capacitance (*Cdl*) was calculated to be 0.03875 mF/cm². Although this value is modest compared to highly porous OER catalysts, it is perfectly consistent with the requirements for HER catalysts, where the kinetics are predominantly governed by charge transfer efficiency rather than massive surface area. Compared to the specific capacitance of a standard flat electrode (30 μF/cm²), the calculated roughness factor was approximately 1.29. Given the electrode's geometric area, the corresponding ECSA was found to be ~ 0.026 cm². This moderate yet effective active surface area provides sufficient accessible sites for proton reduction without hindering the rapid release of generated H_2 bubbles.

Further electrochemical characterization, presented in the Nyquist plot in Fig. 5d, confirmed the superior conductivity of the PANI@ZnNA-MOF electrode. The charge transfer resistance (*Rct*), which corresponds to the diameter of the semicircle, was significantly reduced for the modified electrode. While the bare GCE exhibited a high *Rct* of ~ 117 kΩ, the PANI@ZnNA-MOF electrode displayed a remarkably lower *Rct* of 41 kΩ. This dramatic reduction in charge transfer resistance points to excellent intrinsic electrical conductivity and fast electron transfer kinetics at the electrode-electrolyte interface, which is crucial for efficient HER activity.

The durability of the PANI@ZnNA-MOF electrocatalyst was rigorously evaluated via a 5000-second chronopotentiometry test at a constant current density of 10 mA/cm² (Fig. 5e). The catalyst exhibited outstanding electrochemical stability, maintaining a stable operating potential of ~ 1.8 V vs. RHE throughout the entire test with virtually no potential shift or degradation. This further suitability of the developed PANI@Zn-NA-MOF for clean hydrogen generation.

4. Conclusion

This study demonstrates a simple and economically viable synthesis route for fabricating a novel non-noble metal bifunctional electrocatalyst, PANI@ZnNA-MOF, based on a polyaniline-wrapped zinc-based metal-organic framework. The material was comprehensively characterized and exhibited exceptional electrocatalytic activity toward both the oxygen evolution reaction (OER) and the hydrogen evolution reaction (HER) in alkaline media.

For the OER, the catalyst delivered a current density of 10 mA/cm² at an overpotential of ~ 270 mV, which is highly competitive with recently reported transition-metal-based OER catalysts, such as NiFe-LDH and Co_3O_4, which typically require overpotentials of 280–350 mV. The superior OER activity is attributed to its exceptionally high double-layer capacitance (329.4 mF/cm²) and low charge transfer resistance (~ 6,000 Ω), indicating a massive electrochemically active surface area (ECSA) and rapid electron transfer kinetics.

For the HER, the same catalyst required only ~ 210 mV of overpotential to reach 10 mA/cm², outperforming many recently published non-precious metal HER catalysts (e.g., MoS_2-based systems, which typically show overpotentials of 250–300 mV). The HER performance was supported by a moderate yet optimal *Cdl* of 0.03875 mF/cm²—a value strikingly comparable to that of commercial Pt/C—and an exceptionally low *Rct* of 41 kΩ, confirming fast proton reduction kinetics with minimal charge transfer barriers.

Most notably, the PANI@ZnNA-MOF catalyst exhibited outstanding long-term durability for both reactions. During rigorous 5000-second chronopotentiometry tests, the electrode maintained a highly stable operating potential with virtually no potential shift or degradation, a stability performance that surpasses numerous recently reported noble-metal-free catalysts which often suffer from significant performance decay within the first few hours.

In conclusion, the PANI@ZnNA-MOF composite presents itself as a highly promising, cost-effective, and exceptionally durable alternative to noble-metal-based catalysts. Its competitive activity, combined with its remarkable stability, positions it as a strong candidate for advancing sustainable, large-scale clean hydrogen production technologies and next-generation electrochemical energy conversion systems.

Declarations

Author Contribution

HSA did expermental design , experimental and characterization, HM M and K A A validation of results and writing first draft while AK di write first draft and reviwing final draft of the manuscript.

Data Availability

Data will be available on requets by the editor.

References

1. S. Chu, A. Majumdar, Opportunities and challenges for a sustainable energy future. Nature. **488**, 294–303 (2012). https://doi.org/10.1038/nature11475

2. A. John, Turner. Sustainable Hydrogen Production.*Science*305,972–974(2004). 10.1126/science.1103197
3. Z.W. eh, J. Kibsgaard, C.F. Dickens, I. Chorkendorff, J.K. Nørskov, T.F. Jaramillo, Combining theory and experiment in electrocatalysis: Insights into materials design. Science. 2017;355(6321):eaad4998. 10.1126/science.aad4998. PMID: 28082532
4. A.K. Vannucci, L. Alibabaei, M.D. Losego, J.J. Concepcion, B. Kalanyan, G.N. Parsons, T.J. Meyer, Crossing the divide between homogeneous and heterogeneous catalysis in water oxidation. Proc. Natl. Acad. Sci. U S A **110**(52), 20918–20922 (2013). 10.1073/pnas.1319832110. Epub 2013 Nov 25. PMID: 24277824; PMCID: PMC3876227
5. J.Y. Yang, S.E. Smith, T. Liu, W.G. Dougherty, W.A. Hoffert, W.S. Kassel, M. Rakowski DuBois, D.L. DuBois, R.M. Bullock, Two pathways for electrocatalytic oxidation of hydrogen by a nickel bis(diphosphine) complex with pendant amines in the second coordination sphere. J. Am. Chem. Soc. **135**(26), 9700–9712 (2013). 10.1021/ja400705a. . Epub 2013 Jun 20. PMID: 23631473
6. C.C. McCrory, S. Jung, I.M. Ferrer, S.M. Chatman, J.C. Peters, T.F. Jaramillo, Benchmarking hydrogen evolving reaction and oxygen evolving reaction electrocatalysts for solar water splitting devices. J. Am. Chem. Soc. **137**(13), 4347–4357 (2015). 10.1021/ja510442p. . Epub 2015 Mar 25. PMID: 25668483
7. I. Roger, M.A. Shipman, M.D. Symes, Earth-abundant catalysts for electrochemical and photoelectrochemical water splitting. Nat. Rev. Chem. **1**, 0003 (2017). https://doi.org/10.1038/s41570-016-0003
8. T. Reier, M. Oezaslan, P. Strasser, Electrocatalytic Oxygen Evolution Reaction (OER) on Ru, Ir, and Pt Catalysts: A Comparative Study of Nanoparticles and Bulk Materials. ACS Catal. **2**, 1765–1772 (2012). https://doi.org/10.1021/cs3003098
9. W. Sheng, Z. Zhuang, M. Gao, J. Zheng, J.G. Chen, Y. Yan, Correlating hydrogen oxidation and evolution activity on platinum at different pH with measured hydrogen binding energy. Nat. Commun. **6**, 5848 (2015). https://doi.org/10.1038/ncomms6848
10. M.-I. Jamesh, X. Sun, Recent progress on earth abundant electrocatalysts for oxygen evolution reaction (OER) in alkaline medium to achieve efficient water splitting – A review. J. Power Sources. **400**, 31–68 (2018). https://doi.org/10.1016/j.jpowsour.2018.07.125
11. J. Kibsgaard, I. Chorkendorff, Considerations for the scaling-up of water splitting catalysts. Nat. Energy. **4**, 430–433 (2019). https://doi.org/10.1038/s41560-019-0407-1
12. N.-T. Suen, S.-F. Hung, Q. Quan, N. Zhang, Y.-J. Xu, H.M. Chen, Electrocatalysis for the oxygen evolution reaction: recent development and future perspectives. Chem. Soc. Rev. **46**, 337–365 (2017). https://doi.org/10.1039/C6CS00328A
13. B. You, Y. Sun, Innovative Strategies for Electrocatalytic Water Splitting. Acc. Chem. Res. **51**, 1571–1580 (2018). https://doi.org/10.1021/acs.accounts.8b00002
14. M.E.G. Lyons, M.P. Brandon, The significance of electrochemical impedance spectra recorded during active oxygen evolution for oxide covered Ni, Co and Fe electrodes in alkaline solution. J.

Electroanal. Chem. **631**, 62–70 (2009). https://doi.org/10.1016/j.jelechem.2009.03.019

15. E. Fabbri, A. Habereder, K. Waltar, R. Kötz, T.J. Schmidt, Developments and perspectives of oxide-based catalysts for the oxygen evolution reaction. Catal. Sci. Technol. **4**, 3800–3821 (2014). https://doi.org/10.1039/C4CY00669K
16. F. Song, X. Hu, Exfoliation of layered double hydroxides for enhanced oxygen evolution catalysis. Nat. Commun. **5**, 4477 (2014). https://doi.org/10.1038/ncomms5477
17. M. Ledendecker, S. Krick Calderón, C. Papp, H. Steinrück, M. Antonietti, M. Shalom, The Synthesis of Nanostructured Ni 5 P 4 Films and their Use as a Non-Noble Bifunctional Electrocatalyst for Full Water Splitting, Angew. Chemie Int. Ed. **54**, 12361–12365 (2015). https://doi.org/10.1002/anie.201502438
18. N. Muzaffar, A.M. Afzal, H.H. Hegazy, M.W. Iqbal, Recent advances in two-dimensional metal-organic frameworks as an exotic candidate for the evaluation of redox-active sites in energy storage devices. J. Energy Storage. **64**, 107142 (2023). https://doi.org/10.1016/j.est.2023.107142
19. H. Wang, J.-M. Lee, Recent advances in structural engineering of MXene electrocatalysts. J. Mater. Chem. A **8**, 10604–10624 (2020). https://doi.org/10.1039/D0TA03271A
20. Z. Zhang, J. Liu, J. Wang, Q. Wang, Y. Wang, K. Wang, Z. Wang, M. Gu, Z. Tang, J. Lim, T. Zhao, F. Ciucci, Single-atom catalyst for high-performance methanol oxidation. Nat. Commun. **12**, 5235 (2021). https://doi.org/10.1038/s41467-021-25562-y
21. D. Kong, H. Wang, J.J. Cha, M. Pasta, K.J. Koski, J. Yao, Y. Cui, Synthesis of MoS 2 and MoSe 2 Films with Vertically Aligned Layers. Nano Lett. **13**, 1341–1347 (2013). https://doi.org/10.1021/nl400258t
22. J. Zhang, T. Wang, D. Pohl, B. Rellinghaus, R. Dong, S. Liu, X. Zhuang, X. Feng, Interface Engineering of MoS 2 /Ni 3 S 2 Heterostructures for Highly Enhanced Electrochemical Overall-Water-Splitting Activity, Angew. Chemie Int. Ed. **55**, 6702–6707 (2016). https://doi.org/10.1002/anie.201602237
23. H. Vrubel, X. Hu, Molybdenum Boride and Carbide Catalyze Hydrogen Evolution in both Acidic and Basic Solutions. Angew Chemie Int. Ed. **51**, 12703–12706 (2012). https://doi.org/10.1002/anie.201207111
24. M.W. Louie, A.T. Bell, An Investigation of Thin-Film Ni–Fe Oxide Catalysts for the Electrochemical Evolution of Oxygen. J. Am. Chem. Soc. **135**, 12329–12337 (2013). https://doi.org/10.1021/ja405351s
25. J. Tian, Q. Liu, A.M. Asiri, X. Sun, Self-Supported Nanoporous Cobalt Phosphide Nanowire Arrays: An Efficient 3D Hydrogen-Evolving Cathode over the Wide Range of pH 0–14. J. Am. Chem. Soc. **136**, 7587–7590 (2014). https://doi.org/10.1021/ja503372r
26. S. Anantharaj, S.R. Ede, K. Karthick, S. Sam Sankar, K. Sangeetha, P.E. Karthik, S. Kundu, Precision and correctness in the evaluation of electrocatalytic water splitting: revisiting activity parameters with a critical assessment. Energy Environ. Sci. **11**, 744–771 (2018). https://doi.org/10.1039/C7EE03457A
27. L. Jiao, H.-L. Jiang, Metal-organic frameworks for catalysis: Fundamentals and future prospects. Chin. J. Catal. **45**, 1–5 (2023). https://doi.org/10.1016/S1872-2067(22)64193-7

28. Q. Wang, D. Astruc, Nanocatalysis, Chem. Rev. **120**, 1438–1511 (2020). https://doi.org/10.1021/acs.chemrev.9b00223
29. H. Furukawa, K.E. Cordova, M. O'Keeffe, O.M. Yaghi, The Chemistry and Applications of Metal-Organic Frameworks, Science (80-.). 341 (2013). https://doi.org/10.1126/science.1230444
30. K. Shen, L. Zhang, X. Chen, L. Liu, D. Zhang, Y. Han, J. Chen, J. Long, R. Luque, Y. Li, B. Chen, Ordered macro-microporous metal-organic framework single crystals, Science (80-.). 359 (2018) 206–210. https://doi.org/10.1126/science.aao3403
31. M. Zhao, K. Yuan, Y. Wang, G. Li, J. Guo, L. Gu, W. Hu, H. Zhao, Z. Tang, Metal–organic frameworks as selectivity regulators for hydrogenation reactions. Nature. **539**, 76–80 (2016). https://doi.org/10.1038/nature19763
32. S.-M. Shih, L.-C. Lin, Water Adsorption in Metal–Organic Frameworks: Characteristics, Mechanisms, and Structure–Property Relationships. J. Am. Chem. Soc. **147**, 34791–34803 (2025). https://doi.org/10.1021/jacs.5c10686
33. T. Zhang, W. Lin, Metal–organic frameworks for artificial photosynthesis and photocatalysis. Chem. Soc. Rev. **43**, 5982–5993 (2014). https://doi.org/10.1039/C4CS00103F
34. N. Kornienko, Y. Zhao, C.S. Kley, C. Zhu, D. Kim, S. Lin, C.J. Chang, O.M. Yaghi, P. Yang, Metal–Organic Frameworks for Electrocatalytic Reduction of Carbon Dioxide. J. Am. Chem. Soc. **137**, 14129–14135 (2015). https://doi.org/10.1021/jacs.5b08212
35. K.-S. Lin, A.K. Adhikari, C.-N. Ku, C.-L. Chiang, H. Kuo, Synthesis and characterization of porous HKUST-1 metal organic frameworks for hydrogen storage. Int. J. Hydrogen Energy. **37**, 13865–13871 (2012). https://doi.org/10.1016/j.ijhydene.2012.04.105
36. I. Stassen, N.C. Burtch, A.A. Talin, P. Falcaro, M.D. Allendorf, R. Ameloot, Correction: An updated roadmap for the integration of metal–organic frameworks with electronic devices and chemical sensors. Chem. Soc. Rev. **46**, 3853–3853 (2017). https://doi.org/10.1039/C7CS90048A
37. C.A. Downes, S.C. Marinescu, Electrocatalytic Metal–Organic Frameworks for Energy Applications, ChemSusChem 10 (2017) 4374–4392. https://doi.org/10.1002/cssc.201701420
38. W. Chen, Z. Liu, J. Tian, J. Li, J. Ma, X. Cheng, G. Li, Building Congested Ketone: Substituted Hantzsch Ester and Nitrile as Alkylation Reagents in Photoredox Catalysis. J. Am. Chem. Soc. **138**, 12312–12315 (2016). https://doi.org/10.1021/jacs.6b06379
39. M. Liu, Y. Peng, W. Chen, S. Cao, S. Chen, F. Lu Meng, Y. Jin, C.-C. Hou, R. Zou, Q. Xu, Metal-organic frameworks for carbon-neutral catalysis: State of the art, challenges, and opportunities. Coord. Chem. Rev. **506**, 215726 (2024). https://doi.org/10.1016/j.ccr.2024.215726
40. A. Zarkov, Sol–Gel Technology Applied to Materials Science: Synthesis, Characterization and Applications. Mater. (Basel). **17**, 462 (2024). https://doi.org/10.3390/ma17020462
41. H.-Y. Li, S.-N. Zhao, S.-Q. Zang, J. Li, Functional metal–organic frameworks as effective sensors of gases and volatile compounds. Chem. Soc. Rev. **49**, 6364–6401 (2020). https://doi.org/10.1039/C9CS00778D

42. Y. Zhou, Z. Zhan, Conjugated Microporous Polymers for Heterogeneous Catalysis. Chem. – Asian J. **13**, 9–19 (2018). https://doi.org/10.1002/asia.201701107
43. Y. Xu, S. Jin, H. Xu, A. Nagai, D. Jiang, Conjugated microporous polymers: design, synthesis and application. Chem. Soc. Rev. **42**, 8012 (2013). https://doi.org/10.1039/c3cs60160a
44. C. Zhang, B.-H. Wu, M.-Q. Ma, Z. Wang, Z.-K. Xu, Ultrathin metal/covalent–organic framework membranes towards ultimate separation. Chem. Soc. Rev. **48**, 3811–3841 (2019). https://doi.org/10.1039/C9CS00322C
45. J. Li, X. Wang, G. Zhao, C. Chen, Z. Chai, A. Alsaedi, T. Hayat, X. Wang, Metal–organic framework-based materials: superior adsorbents for the capture of toxic and radioactive metal ions. Chem. Soc. Rev. **47**, 2322–2356 (2018). https://doi.org/10.1039/C7CS00543A
46. H. Li, L. Wang, G. Yu, Covalent organic frameworks: Design, synthesis, and performance for photocatalytic applications. Nano Today. **40**, 101247 (2021). https://doi.org/10.1016/j.nantod.2021.101247
47. R.R. Salunkhe, Y.V. Kaneti, Y. Yamauchi, Metal–Organic Framework-Derived Nanoporous Metal Oxides toward Supercapacitor Applications: Progress and Prospects. ACS Nano. **11**, 5293–5308 (2017). https://doi.org/10.1021/acsnano.7b02796
48. R. Ciriminna, A. Fidalgo, V. Pandarus, F. Béland, L.M. Ilharco, M. Pagliaro, The Sol–Gel Route to Advanced Silica-Based Materials and Recent Applications. Chem. Rev. **113**, 6592–6620 (2013). https://doi.org/10.1021/cr300399c
49. Z. Wu, K. Parvez, X. Feng, K. Müllen, Graphene-based in-plane micro-supercapacitors with high power and energy densities. Nat. Commun. **4**, 2487 (2013). https://doi.org/10.1038/ncomms3487
50. Z.-G. Gu, J. Zhang, Epitaxial growth and applications of oriented metal–organic framework thin films. Coord. Chem. Rev. **378**, 513–532 (2019). https://doi.org/10.1016/j.ccr.2017.09.028
51. A.C. Pierre, *Introduction to Sol-Gel Processing* (Springer International Publishing, Cham, 2020). https://doi.org/10.1007/978-3-030-38144-8
52. L. Kaßner, J. Kronawitt, D. Klimm, A. Seifert, S. Spange, Molecular aspects on the amino acid-mediated sol–gel process of tetramethoxysilane in water. J. Sol-Gel Sci. Technol. **90**, 250–262 (2019). https://doi.org/10.1007/s10971-019-04930-7
53. B.M. Omkaramurthy, G. Krishnamurthy, S. Foro, Synthesis and characterization of mesoporous crystalline copper metal–organic frameworks for electrochemical energy storage application. SN Appl. Sci. **2**, 342 (2020). https://doi.org/10.1007/s42452-020-2051-6
54. K. Nakamoto, *Infrared and Raman Spectra of Inorganic and Coordination Compounds* (Wiley, 2008). https://doi.org/10.1002/9780470405888
55. I. Sapurina, J. Stejskal, The mechanism of the oxidative polymerization of aniline and the formation of supramolecular polyaniline structures. Polym. Int. **57**, 1295–1325 (2008). https://doi.org/10.1002/pi.2476
56. A. Yelil Arasi, J. Juliet Latha Jeyakumari, B. Sundaresan, V. Dhanalakshmi, R. Anbarasan, The structural properties of Poly(aniline)—Analysis via FTIR spectroscopy, Spectrochim. Acta Part. Mol.

Biomol. Spectrosc. **74**, 1229–1234 (2009). https://doi.org/10.1016/j.saa.2009.09.042

57. S. Bhadra, D. Khastgir, N.K. Singha, J.H. Lee, Progress in preparation, processing and applications of polyaniline. Prog Polym. Sci. **34**, 783–810 (2009). https://doi.org/10.1016/j.progpolymsci.2009.04.003
58. S. Rojas, A. Rodríguez-Diéguez, P. Horcajada, Metal–Organic Frameworks in Agriculture. ACS Appl. Mater. Interfaces. **14**, 16983–17007 (2022). https://doi.org/10.1021/acsami.2c00615
59. X. Li, X. Yang, H. Xue, H. Pang, Q. Xu, Metal–organic frameworks as a platform for clean energy applications, EnergyChem 2 (2020) 100027. https://doi.org/10.1016/j.enchem.2020.100027
60. S. Wang, L. Zhao, J. Li, X. Tian, X. Wu, L. Feng, High valence state of Ni and Mo synergism in NiS2-MoS2 hetero-nanorods catalyst with layered surface structure for urea electrocatalysis. J. Energy Chem. **66**, 483–492 (2022). https://doi.org/10.1016/j.jechem.2021.08.042
61. M. Li, Y. Gu, Y. Chang, X. Gu, J. Tian, X. Wu, L. Feng, Iron doped cobalt fluoride derived from CoFe layered double hydroxide for efficient oxygen evolution reaction. Chem. Eng. J. **425**, 130686 (2021). https://doi.org/10.1016/j.cej.2021.130686
62. M. Zha, C. Pei, Q. Wang, G. Hu, L. Feng, Electrochemical oxygen evolution reaction efficiently boosted by selective fluoridation of FeNi3 alloy/oxide hybrid. J. Energy Chem. **47**, 166–171 (2020). https://doi.org/10.1016/j.jechem.2019.12.008
63. Z. Liu, C. Zhang, H. Liu, L. Feng, Efficient synergism of NiSe2 nanoparticle/NiO nanosheet for energy-relevant water and urea electrocatalysis. Appl. Catal. B Environ. **276**, 119165 (2020). https://doi.org/10.1016/j.apcatb.2020.119165
64. T.N. Myasoedova, O.V. Nedoedkova, R. Kalusulingam, Y.V. Popov, A.S. Mikheykin, A.S. Konstantinov, L. Zhengyou, T.S. Mikhailova, V.A. Shmatko, G.E. Yalovega, Fabrication of Ni-Polyaniline/Graphene Oxide Composite Electrode with High Capacitance and Water Splitting Activity, ChemPhysChem 25 (2024). https://doi.org/10.1002/cphc.202300795
65. S. Lahkar, R. Brahma, S.K. Dolui, Iron Doped Titania/Polyaniline Composite: An Efficient Electrocatalyst for Hydrogen Evolution Reaction in Acidic Medium. Catal. Res. **03**, 1–18 (2023). https://doi.org/10.21926/cr.2301002
66. N. Kareem, I. Karim, S.A. Alsalhi, J. Makasana, M.M. Rekha, G.S. Kumar, M.A. Al-Anber, S.N. Das, R.R. Chaudhary, A. Kumar, A.D. Oza, CuFe2O4 embedded on polyaniline nanosheet a promising electrocatalyst for OER. J. Indian Chem. Soc. **102**, 101759 (2025). https://doi.org/10.1016/j.jics.2025.101759
67. S. Moradi-Alavian, A. Kazempour, H. Ashassi-Sorkhabi, E. Asghari, A. Mehrdad, Positional effects of chlorine-substituted polyaniline reinforced with feco2s4 on HER and supercapacitor performance. Sci. Rep. **15**, 33606 (2025). https://doi.org/10.1038/s41598-025-18998-5
68. J. Milikić, J. Mišurović, L. Rakočević, I.A. Pašti, G. Ćirić-Marjanović, B. Šljukić, Polyaniline prepared by Fe3O4 catalysed eco-friendly synthesis as electrocatalyst for efficient water electrolysis. J. Electrochem. Sci. Eng. **15**, 2438 (2024). https://doi.org/10.5599/jese.2438

Figures

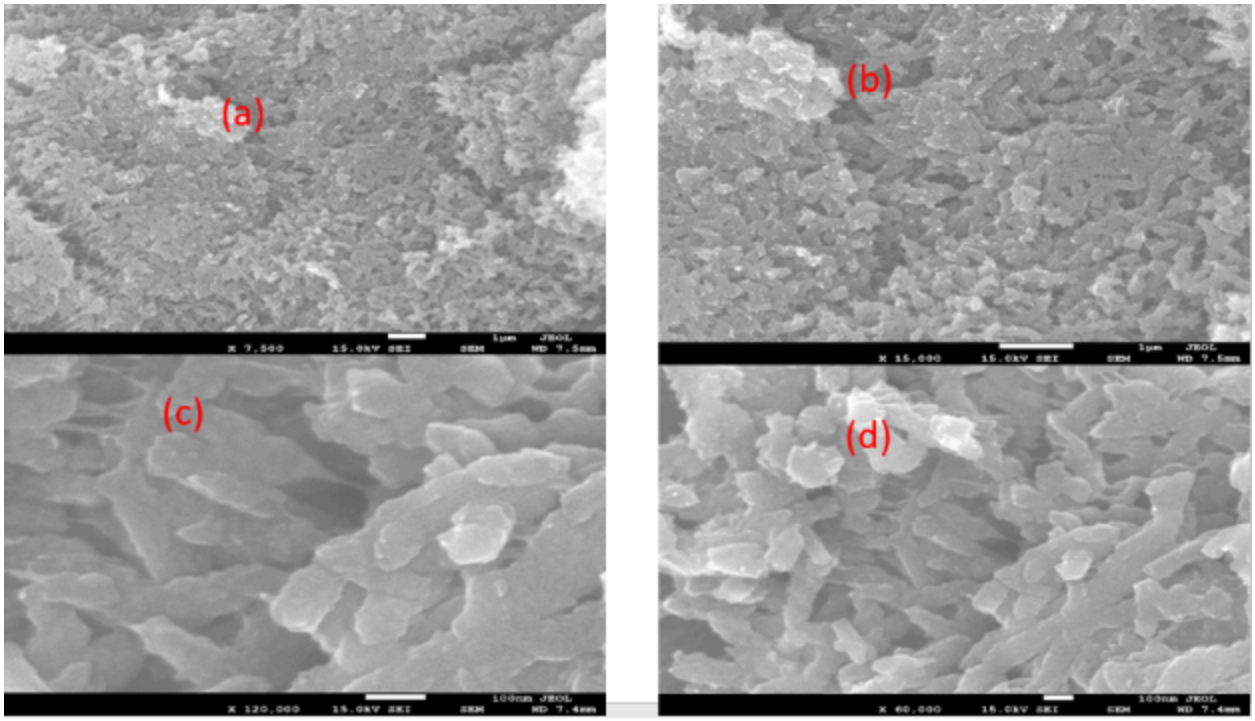

Figure 1

Scanning electron microscope (SEM) image of PANI (a, b) and PANI@ZnNA-MOF (c, d) with different magnifications.

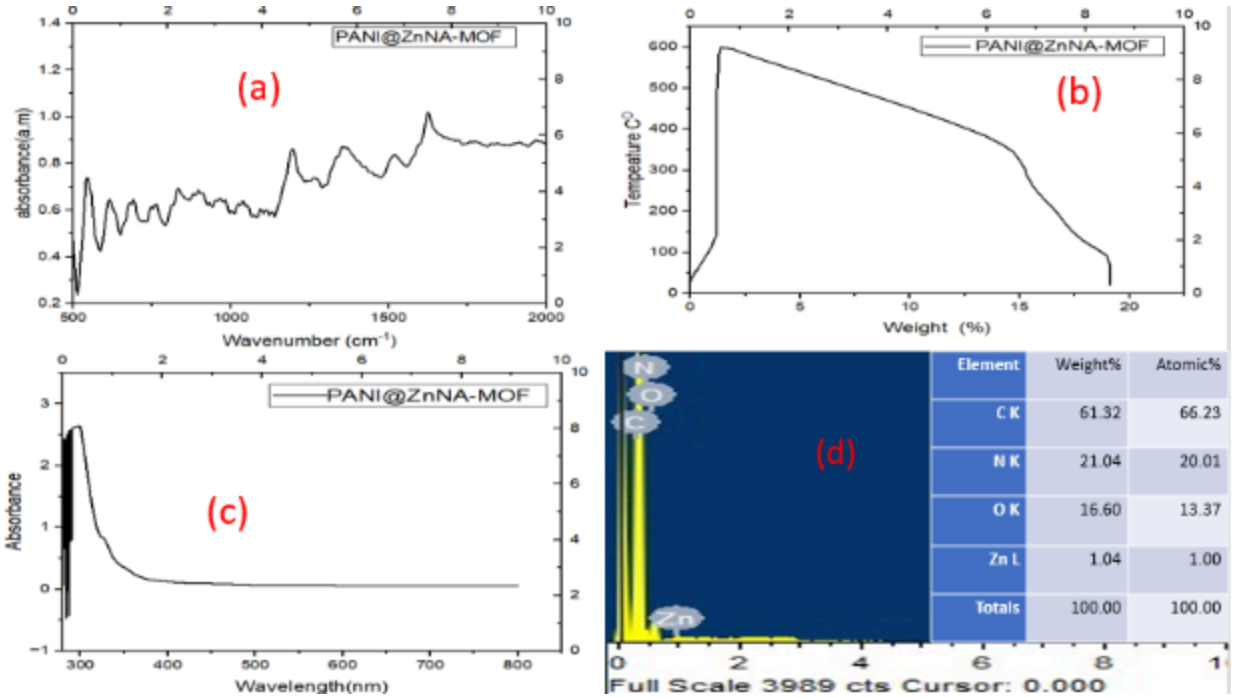

Figure 2

(a) (FTIR) spectrum of PANI@ZnNA-MOF.(b) (TGA) of PANI@ZnNA-MOF (c) (UV) spectrum of PANI@ZnNA-MOF, while d) showing EDX of PANI@ZnNA-MOF.

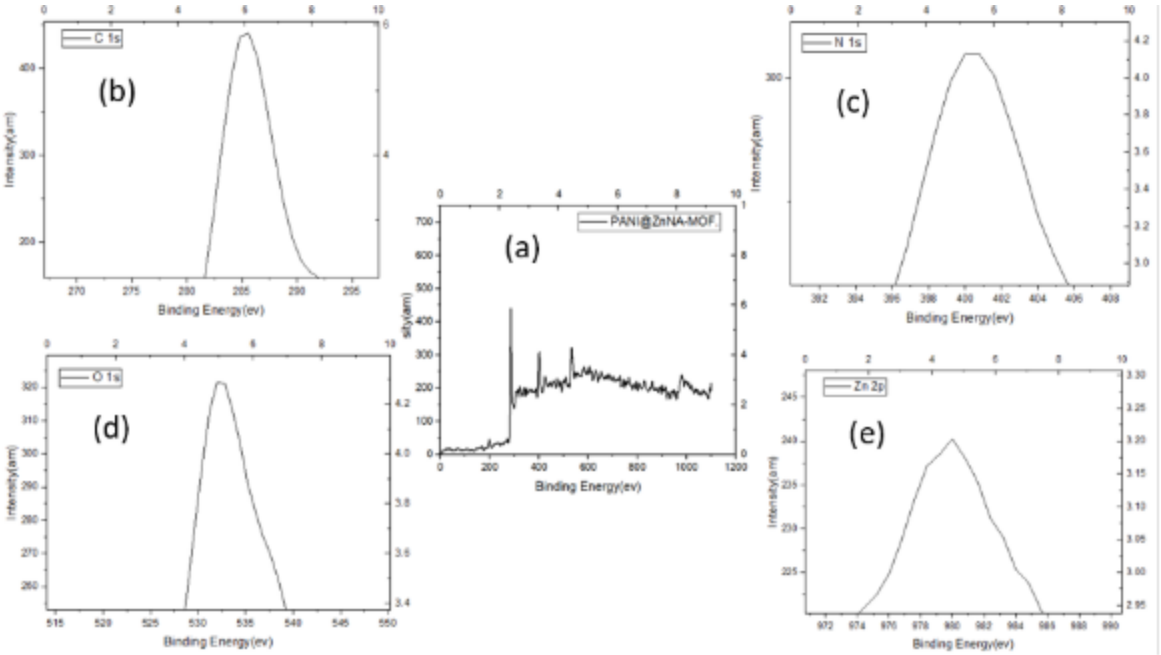

Figure 3

(a) shows XPS of PANI@ZnNA-MOF composite while b) C1s streaching vibration; c) N1s; d) O1s and e) Zn 2p

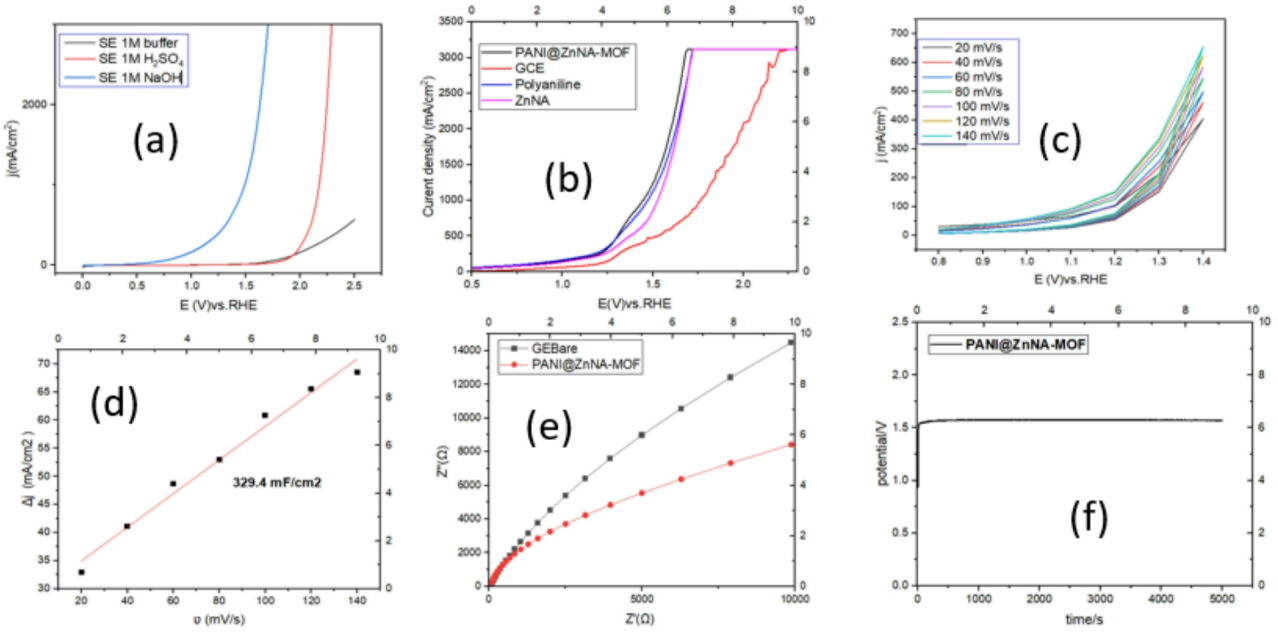

Figure 4

OER studies (a) Supporting electrolyte optimization (b) Control study. (c) Effect of scan rate on OER. (d) Double layer capacitance (Cdl) determination (e) EIS spectrum of PANI@CuNA-MOF (f) Stability chronopotentiometry

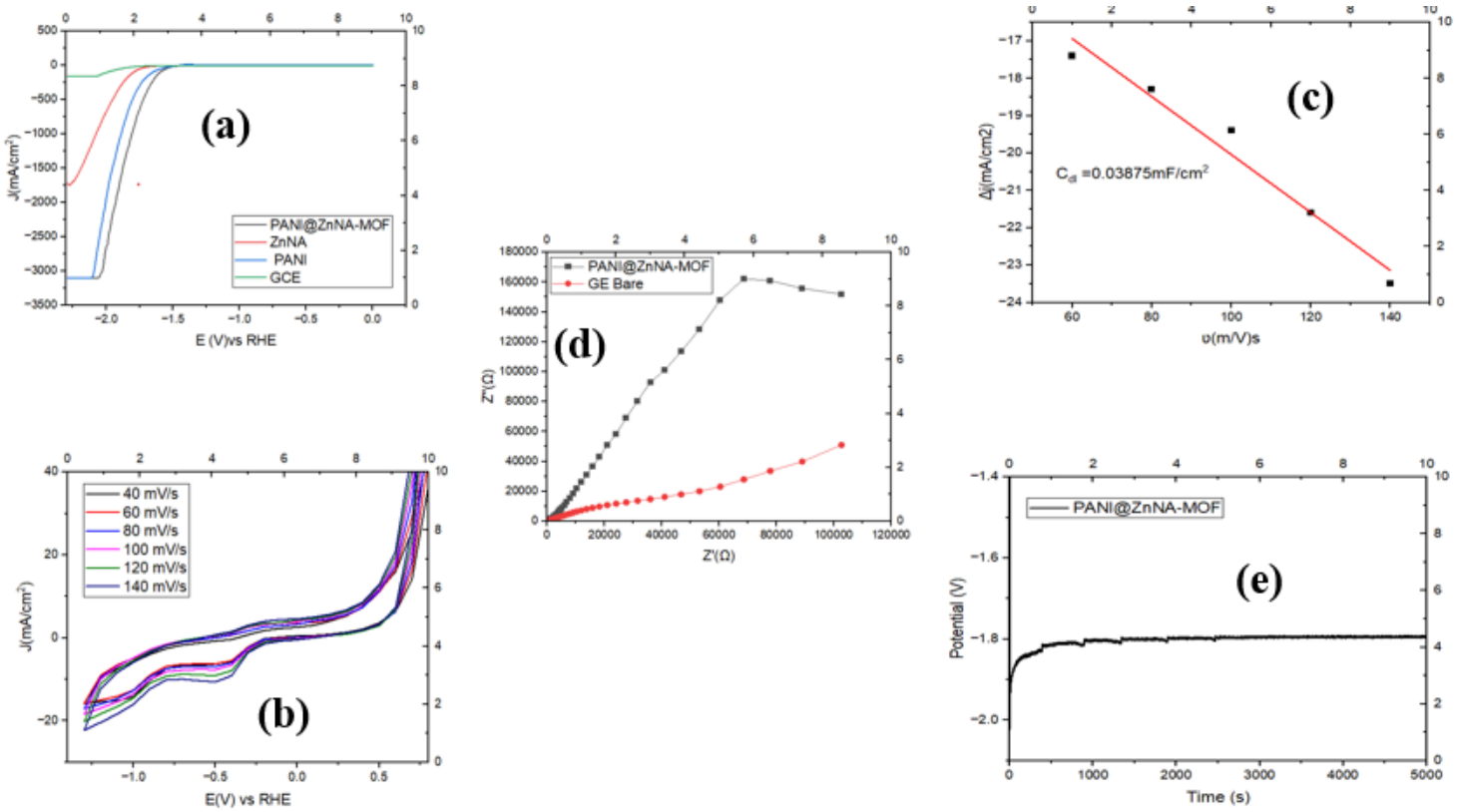

Figure 5

HER reaction studies (a) Control study. (b) Effect of scan rate on HER. (c) Double layer capacitance (Cdl) determination (d) EIS spectrum of PANI@CuNA-MOF (e) Stability chronopotentiometry.